Geoscience Letters

RESEARCH LETTER

Open Access

The simulation of the Indo-Pacific warm pool SST warming trend in CMIP5 and CMIP6

Wenrong Bai[1,2,4], Hailong Liu[2,3*], Pengfei Lin[2,4] and Hongyan Shen[5]

Abstract

This paper evaluates Indo-Pacific warm pool (IPWP) sea surface temperature (SST) warming biases of Coupled Model Intercomparison Project Phase 5 (CMIP5) and CMIP6. The IPWP warming trend in the CMIP5 multi-model ensemble (MME) is closer to observation than in CMIP6 MME, but the IPWP expanding trend is the opposite. There is no qualitative improvement in the simulation of IPWP warming from CMIP5 to CMIP6. In addition, four metrics were used to investigate the performance of Indo-Pacific region warming trends in all models. CMIP6 models perform better than CMIP5 with smaller root mean square error and bias in MME and higher skill scores in MME and top models, which is tightly linked to their better performance in simulating associated physical processes in CMIP6 models. IPWP warming biases are mainly attributed to the combined effects of positive atmospheric process biases and negative ocean dynamics term biases. The positive atmospheric process biases are primarily related to the shortwave radiation and latent heat flux from atmospheric forcing, the latter of which can be attributed to the biases in surface wind fields. Compared with CMIP5 models, the IPWP warming simulated by CMIP6 models is weaker, related to the less robust atmospheric processes and the shallower thermocline anomalies simulated by CMIP6.

Introduction

The Indo-Pacific warm pool (IPWP) is commonly defined as the Indo-Pacific domain (30° S to 30° N and 40° E to 135° W) with sea surface temperature (SST) greater than 28 °C (Clement et al. 2005; Kim et al. 2012; Picaut et al. 1996; Wyrtki 1989). The high SST in the IPWP promotes strong convective motions in the atmosphere, releasing large amounts of latent heat (Spencer 1993), driving the Hadley and Walker circulations, and affecting regional and global climate change through atmospheric teleconnections (Lindzen and Nigam 1987; Marathe et al. 2021; Numaguti 1995; Seager and Vecchi 2010). The IPWP is also a key pathway for the return of large global oceanic conveyor belts from the surface to the Atlantic Ocean, with potential impacts on the global ocean (Banks and Bindoff 2003; Hu et al. 2015; Ma et al. 2016; Wienders et al. 2000).

The IPWP continues to warm and expand in the context of global warming (Bai et al. 2022; Cravatte et al. 2009; Rao et al. 2012; Weller et al. 2016; Williams and Funk 2011), with a twofold expansion of the IPWP during 1981–2018 compared to the 1900–1980 period (Roxy et al. 2019). Climate system models are a powerful tool for studying IPWP SST changes (Eyring et al. 2016). However, there are some uncertainties in the IPWP SST simulations and projections due to the tropical bias in the models (Cai and Cowan 2013; Hayashi et al. 2021; Jin et al. 2023; Li and Xie 2012; Si et al. 2021; Wang et al. 2021; Yao et al. 2016). For example, the Western Pacific Warm Pool area is small and confined to the equator, and

*Correspondence:
Hailong Liu
lhl@lasg.iap.ac.cn
[1] Beijing Municipal Climate Center, Beijing Meteorological Bureau, Beijing 100089, China
[2] State Key Laboratory of Numerical Modeling for Atmospheric Sciences and Geophysical Fluid Dynamics (LASG), Institute of Atmospheric Physics, Chinese Academy of Sciences, Beijing 100029, China
[3] Laoshan Laboratory, Qingdao 266237, China
[4] College of Earth and Planetary Sciences, University of Chinese Academy of Sciences, Beijing 100049, China
[5] Meteorological Institute of Shaanxi Province, Xi'an 710016, Shaanxi, China

the Indian Ocean Warm Pool is shifted southward (Hu et al. 2017; Park et al. 2021; Sun et al. 2013). The ocean currents and thermal advection biases in Coupled Model Intercomparison Project Phase 5 (CMIP5) influence the shape of the climatological warm pool (Yang et al. 2020). There are still large inter-model spreads in the IPWP intensity and size during the present-day climate in CMIP6 (Kug et al. 2023; Liu and Grise 2023). In addition, almost all CMIP5/6 models can reproduce the IPWP SST warming, but the models tend to underestimate the warming trend, with better performance in reproducing Indian Ocean SST warming trends in CMIP5 (Li and Su 2020).

The formation of SST biases involves several physical processes. The climatological SST warm bias in the equatorial western Indian Ocean and the cold bias in the equatorial southeastern Indian Ocean are related to the shallow thermocline and easterly wind anomalies in the tropical southeastern Indian Ocean, and the Bjerknes positive feedback enhances this latitudinal SST gradient biases (Cai and Cowan 2013; McKenna et al. 2020; Wang et al. 2017). Compared to the CMIP5 model, the equatorial southeastern Indian Ocean thermocline simulated by the CMIP6 model remains over-tilted, which can underestimate future increases in SST variability (Wang et al. 2021). The equatorial western Pacific Ocean warm bias is associated with low precipitation in the Western Pacific Warm Pool and eastward flow bias caused by the excessive e equatorial Pacific cold tongue (Li et al. 2015, 2016). Positive cloud-radiation negative feedback bias in the central Pacific can cause SST warm bias in the Central and Western Pacific and SST cold bias in the Eastern Pacific (Ying and Huang 2016).

Although CMIP6 models show better performance than CMIP5 in reproducing globally averaged climatological SST (Zhang et al. 2023a), the spatial distribution and magnitude of regional biases in CMIP6 are similar to those of the CMIP5 and CMIP3 models (Bock et al. 2020; Flato et al. 2014; Randall et al. 2007). Thus, a systematic assessment of two generations of model simulations for IPWP SST trends modeling is essential. We first evaluate the models' ability to simulate IPWP SST warming in CMIP6 and CMIP5, with a focus on the discussions about whether CMIP6 models have made progress in simulating the IPWP SST warming. We then reveal the fundamental physical mechanisms for IPWP SST warming and investigate the causes of model biases based on the mixed-layer heat budget.

Materials and methods

Observational and model datasets

The monthly mean SST observations used in this paper include (1) the extended reconstructed SST (ERSST) version 5 (Smith et al. 2008); (2) the Hadley Centre Sea Ice and SST (HadISST) version 1.1 (Rayner et al. 2003); (3) the centennial in situ observation based estimates SST (COBESST) version 2 (Hirahara et al. 2014). We use the average of HadISST.v1.1, ERSST.v5, and COBESST2 SSTs as the optimal observational SST estimate (referred to as "observation") to reduce uncertainties among different observational datasets.

Monthly gridded radiation flux data were taken from the ERA5 reanalysis dataset (Hersbach et al. 2020). For radiation flux, we also use JRA55 (Kobayashi et al. 2015) and NCEP (Kalnay et al. 1996) as references. Monthly wind data were taken from the NCEP-NCAR reanalysis dataset (Kalnay et al. 1996). Monthly precipitation data were taken from the JRA55 reanalysis dataset (Kobayashi et al. 2015). We also used monthly sea surface height data compiled with the ORAS5 dataset (Zuo et al. 2017).

We use monthly mean SST, radiation flux, wind, precipitation, and sea surface height data from 40 CMIP6 models (Eyring et al. 2016) and 35 CMIP5 models (Taylor et al. 2012). The simulations from all forcing historical experiments (1950–2005) were analyzed, and only the first realization for each model was used (Table 1).

The observational and models were gridded to a typical 1°×1° grids through bilinear interpolation. Since the historical simulations in CMIP5 models were limited to 2005, the period selected in the study is 1961–2005.

Metrics for the warm pool properties

The Indo-Pacific warm pool is defined as the Indo-Pacific domain (30° S to 30° N and 40° E to 135° W) with an SST higher than 28 °C and divided into Indian and Pacific parts by the 120° E meridian. The intensity and area indexes are calculated by the averaged area-weight SST in the area within the 28 °C isotherms and the area size enclosed by the 28 °C isotherm, respectively. The monthly climatological mean is removed when calculating monthly intensity and area anomaly. Annual mean anomalies are constructed from monthly anomalies for analysis.

We calculate the total root mean square error (RMSE), the pattern correlation coefficients (PCC), and the biases between observations and models to quantitatively estimate the models' ability to simulate Indo-Pacific (30° S–30°N, 40° E–135° W) SST warming. We also calculate the skill scores to identify models skill following Taylor (2001) by the following formula (Hirota et al. 2011; Taylor 2001):

$$\mathrm{TS} = \frac{4 \times (1+R)^2}{\left(\frac{\sigma_m}{\sigma_o} + \frac{\sigma_o}{\sigma_m}\right) \times (1+R_0)^2}, \quad (1)$$

where R denotes the spatial correlation coefficient between the model and the observation. R_0 denotes the

maximum value of R among the selected models. σ_o and σ_m present the standard deviation of the observation and the model, respectively.

Heat budget analysis

Following Xie et al. (2010), the SST tendency equation is written as:

$$C\frac{\partial T'}{\partial t} = Q'_{net} + D'_O, \tag{2}$$

where T' is the SST trend from 1961 to 2005. C is the mixed-layer heat capacity. D'_O is the ocean dynamics term due to three-dimensional advection, mixing, and even entrainment. Q'_{net} is the trend for 45 yr in the net surface heat flux into the ocean (positive downward) and is composed of four physical components: net shortwave radiation Q'_s, net longwave radiationQ'_L, net sensible heat flux Q'_H, and net latent heat flux Q'_E.

At the interdecadal or longer time scales, the SST tendency term is one order smaller than the net sea surface heat flux and ocean dynamics term (Schneider and Fan 2012; Xie et al. 2010). Therefore, the net surface heat flux balances the ocean dynamics term to the first order:

$$D'_O = -Q'_{net}. \tag{3}$$

Q'_E can be decomposed into a Newtonian cooling effect ($Q_E^{O'}$) and atmospheric forcing ($Q_E^{a'}$).$Q_E^{O'}$ is written as:

$$Q_E^{O'} = \frac{\partial Q_E}{\partial T}T' = \alpha\overline{Q_E}T', \tag{4}$$

where $\alpha \approx 0.067\,K^{-1}$ is a coefficient. $\overline{Q_E}$ is the climatological latent heat flux.

$Q_E^{a'}$ is calculated as a residual, and can be further decomposed into wind speed, relative humidity, and stability effects. Likewise, the wind speed effect ($Q_E^{W'}$) is written as:

$$Q_E^{W'} = \frac{\partial Q_E}{\partial W}W' = \frac{\overline{Q_E}W'}{\overline{W}}. \tag{5}$$

$\overline{W}$ is the climatological surface wind speed. W' is the surface wind speed trend.

In conclusion, the mixed-layer heat budget equation can be written as:

$$0 = \left(D'_O + Q'_a\right) - \alpha\overline{Q_E}T'. \tag{6}$$

SST warming pattern formation is mainly attributable to ocean dynamics term (D'_O), atmospheric processes via radiative and turbulent fluxes ($Q'_a = Q'_S + Q'_L - Q'_H - Q_E^{a'}$), and climatological latent heat flux ($\overline{Q_E}$):

$$T' = \frac{\left(Q_a{}' + D_O{}'\right)}{\alpha\overline{Q_E}}. \tag{7}$$

Results

IPWP warming in CMIP5 and CMIP6

The observed SST shows a warming trend except for the subtropical northeastern Pacific Ocean, with a salient warming trend in IPWP (Fig. 1a). The multi-model ensemble (MME) can reproduce the observations with uniform warming throughout the entire basin (Fig. 1b and c). However, the spatial distributions of warming trends in MMEs show apparent differences from the observed pattern. CMIP6 and CMIP5 models share similar bias patterns with prominent cold biases over IPWP, the southern Indian Ocean, and the tropical southeastern Pacific Ocean, and with warm biases over the tropical western Indian Ocean and the subtropical northeastern Pacific Ocean. Both model generations simulate zonally elongated and meridionally narrower IPWP compared with the observation (Fig. 1d and e). CMIP6 MME simulates a weaker SST warming pattern in IPWP compared with CMIP5 (Fig. 1f). We calculate the time series and the linear trends for intensity and area anomalies to evaluate the IPWP warming and expanding biases in CMIP6 and CMIP5 (Fig. S1, Fig. 1g and h). The IPWP warmed and expanded steadily in both observations and CMIP5/6 models. The IPWP warming trend in CMIP5 is 0.29 °C/45 yr, closer to observation (0.34 °C/45 yr) than CMIP6 (0.26 °C/45 yr). The model spreads (5–95% model interval) of CMIP5 tend to be slightly smaller than those of CMIP6 for warm pool intensity (Fig. S1a). However, the IPWP expanding trend in CMIP6 (24.5%/45 yr) is closer to observation (27.9%/45 yr) than in CMIP5 (35.7%/45 yr), and the model spreads of the warm pool area in CMIP6 are smaller than those of CMIP5 (Fig. S1b).

We evaluate how well the models can simulate the magnitude and spatial pattern of Indo-Pacific warming components by taking the RMSE, PCC, and mode biases as metrics (Fig. 2a–c). The simulated IPWP SST warming shows only slight improvement from CMIP5 to CMIP6 regarding the ensemble mean or median (smaller RMSE and bias). The peak value of the CMIP6 is smaller than that of the CMIP5 from the perspective of the inter-model PDF distribution of RMSE and bias, with the overall distribution skewed to the low-value regions. The PCCs in CMIP5 and CMIP6 ensembles are similarly low, indicating that the CMIP6 and CMIP5 MME and most individual members do not well represent the IPWP warming pattern.

We calculate Taylor skill scores (see Eq. (1)) and select six models in CMIP5 and CMIP6 ensembles with the

highest (lowest) skill scores as the high-skill (low-skill) ensemble to quantify the performance of models in reproducing IPWP warming (Fig. 2d and e). The skill scores in the CMIP6 MME (0.39) and high-skill ensemble (0.82) are significantly higher than those in CMIP5 (0.14 and 0.76), but the skill score in CMIP6 low-skill ensemble (0.19) is lower than that in CMIP5 (0.30). This indicates that CMIP6 MME and top models show significant improvement in simulating IPWP warming, but CMIP6 ensembles have larger inter-model spreads compared with CMIP5, with inter-model spread 30% higher than CMIP5. The spatial distribution of IPWP warming in the high-skill ensemble, primarily the CMIP6 high-skill ensemble, can characterize the warming trend in the tropical Southern Indian Ocean well and is closer to observations than that in the low-skill ensemble (Fig. S2).

The mixed-layer heat budget analyses

We analyze the mechanisms and the model biases responsible for IPWP warming and quantify the relative contributions of atmospheric and oceanic processes to IPWP warming based on the mixed-layer heat budget (Fig. 3 and Table 1). Atmospheric forcing in ERA5 heats the Northern Indian Ocean, the maritime continent region, the tropical Southwestern and Northern Pacific. Ocean dynamics term has a similar pattern to atmospheric forcing but with an opposite sign. Atmospheric forcing and ocean dynamics term in IPWP are comparable but have a more substantial magnitude in ocean dynamics term (Table 1). The sum of atmospheric and oceanic processes heats almost the Indo-Pacific basin, with two maximum centers in IPWP and the off-equatorial southeastern basin. The sum of atmospheric and oceanic processes positively contributes to the SST pattern, with a PCC of approximately 0.90. The distribution of Newtonian cooling coefficients also affects the SST warming pattern, as indicated in Eq. (7), and is generally symmetric about the equator, with maxima located in the off-equatorial zones of about 10°–20°S and 10°–20°N. We compare the performance of the ERA5 dataset with two other datasets–JRA55 (Fig. S3) and NCEP (Fig. S4). Results showed that although atmospheric forcing (or ocean dynamics term) exhibits spatial differences over IPWP among different datasets, the sum of atmospheric and oceanic processes shares a similar spatial pattern. Notably, the heating effects of the sum of atmospheric

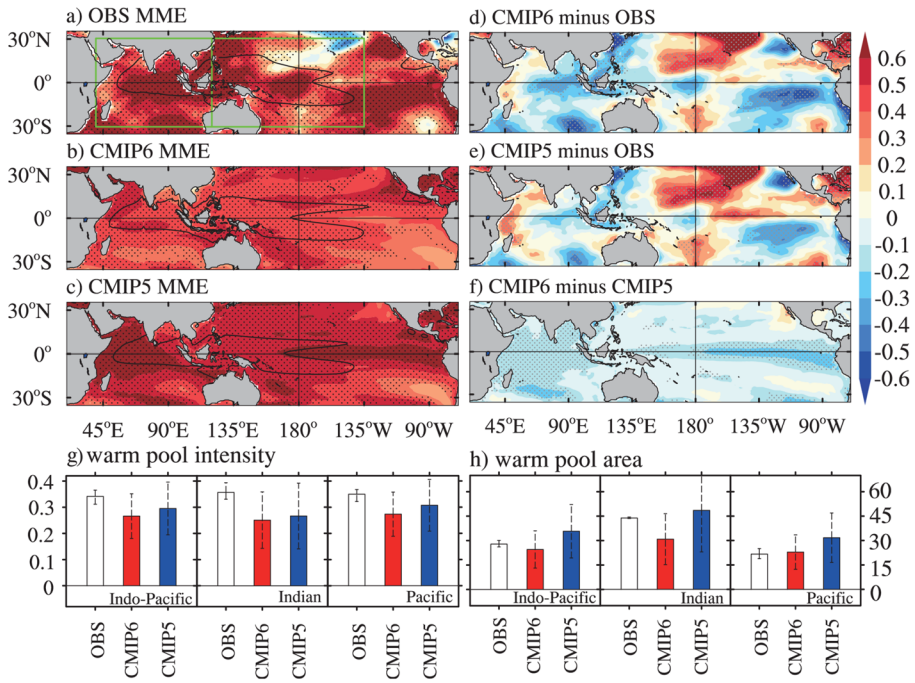

Fig. 1 Spatial distributions of the linear trends of annual mean SST (unit: ℃/45 yr) over the Indo-Pacific during 1961–2005 in the observation (**a**), CMIP6 (**b**), and CMIP5 (**c**) ensemble means. **d** and **e** Biases of CMIP6 (**d**) and CMIP5 (**e**) model simulations against the observations. **f** The difference between CMIP6 and CMIP5 ensemble means. Linear trends of warm pool intensity (**g**, unit: ℃/45 yr) anomalies (relative to the 1951–2005 climatology) and percentage of the area (**h**, unit: %/45 yr) anomalies for observations (white), CMIP6 (red), and CMIP5 (blue) multi-model ensemble means for Indo-Pacific (top), Indian (center), and Pacific (bottom). Black contours in a-c represent climatological 28℃ isotherms. The solid green lines represent the Indo-Pacific warm pool area (**a**). Dots represent the trends statistically significant at the 95% level using a student's *t*-test (**a**–**c**), and the biases are statistically significant at the 95% level (**d**–**f**). Error bars represent 5 to 95% model intervals

and oceanic processes over IPWP are comparable, with the maximum difference between ERA5 and two other datasets less than 1 Wm^{-2}/45 yr.

Compared to reanalysis datasets, CMIP6 and CMIP5 models suffer from atmospheric and oceanic process biases. Atmospheric forcing in models heats the entire Indo-Pacific basin and plays a dominant role, while the ocean dynamics term exerts a more negligible and opposite effect. The sum of atmospheric and oceanic processes presents a maximum center in the off-equatorial zones, which is weakened due to Newtonian cooling coefficients. Therefore, the basin-wide warming is spatially uniform in models. Besides, the heating effects of atmospheric forcing and the sum of atmospheric and oceanic processes in CMIP6 are weaker than those in CMIP5 (Fig. S5).

We also calculate four components of atmospheric forcing: shortwave radiation, longwave radiation, sensible heat flux, and latent heat flux from atmospheric forcing. In ERA5, shortwave radiation cools most of the basin due to intensified water vapor absorption caused by moistening in the lower troposphere (Trenberth and Fasullo 2009). The increase in convective clouds and precipitation owing to IPWP warming reduces shortwave radiation even more. Longwave radiation nearly warms the entire basin due to increased greenhouse gas emissions and water vapor feedback (Du and Xie 2008). Sensible heat flux also warms the basin and exerts a more minor effect. Latent heat flux from atmospheric forcing presents a similar distribution to atmospheric forcing. Among the atmospheric forcings, latent heat flux from atmospheric forcing, longwave radiation, and sensible heat flux are comparable in IPWP warming in ERA5 (Table 1). In CMIP5 and CMIP6 models, shortwave radiation cools the Arabian Sea, Bay of Bengal, South China Sea, and Indonesia regions; longwave radiation, sensible heat flux, and latent heat flux from atmospheric forcing warm the entire basin. Among the atmospheric forcings, latent heat flux from atmospheric forcing plays a dominant role in IPWP warming, followed by longwave radiation, and sensible heat flux is negligible (Table 1).

For IPWP warming biases in CMIP5 and CMIP6 induced by atmospheric forcing, especially by shortwave radiation and latent heat flux from atmospheric forcing (Table 1). The biases of latent heat flux from atmospheric forcing are related to the biases of the near-surface specific humidity variations and wind speed U variations (Zhang et al. 2018). Tropical latent heat flux

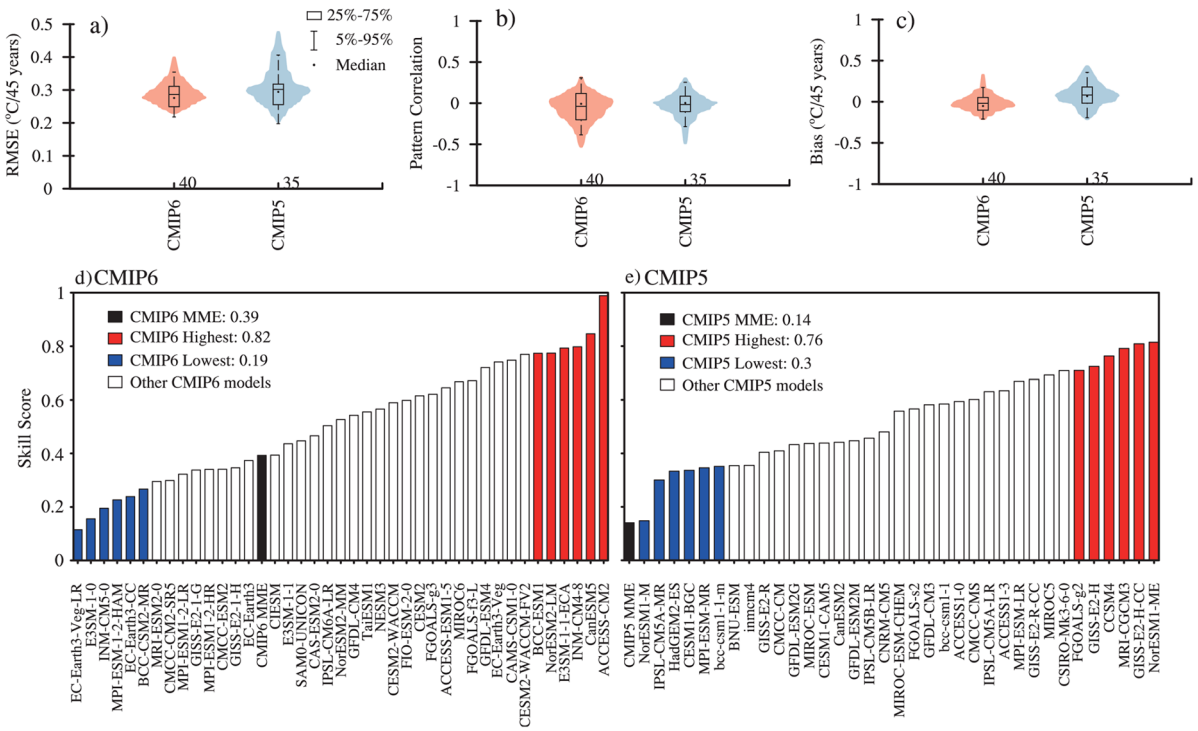

Fig. 2 Root mean square error (**a**, unit: ℃/45 yr), pattern correlation coefficient (**b**), and model bias (**c**, unit: ℃/45 yr) of SST trends during 1961–2005 in Indo-Pacific region (30° S–30° N, 40° E–135° W) in CMIP6 (red) and CMIP5 (blue) models. Box and vertical bar edges represent 25–75% and 5–95% in each CMIP ensemble, and black circles are the medians. Shading indicates density trace. Taylor skill scores of SST trends during 1961–2005 in Indo-Pacific warm pool area in CMIP6 (**d**) and CMIP5 (**e**) models

variations have been more positively connected to wind speed U variations in recent years (Zhang et al. 2023b). We further analyze the wind effect on latent heat flux from atmospheric forcing, which could explain most of the atmospheric term of latent heat flux (Fig. 4). The wind effect on latent heat flux from atmospheric forcing warms the Bay of Bengal, the equatorial eastern Indian Ocean and the dateline area in ERA5, due to reduced climatological wind speed and less evaporation. In addition, the anomalous easterly winds deepen the thermocline (positive SSH anomaly) in the equatorial eastern Indian Ocean, which benefits to enhance thermocline feedback to reduce upwelling and raise SST. In CMIP5 and CMIP6, the wind effect on latent heat flux from atmospheric forcing warms the entire Indian Ocean Warm Pool and north of the equator Pacific. The SST warming signal in the Indian Ocean Warm Pool is consistent with an abnormal anti-symmetric wind pattern, with anomalous easterly occupying most parts of the northern Indian Ocean and northwesterly extending south of the equator, which helps to suppress the climatological wind. The westerly anomalies reduce the prevailing easterly over the western Pacific warm pool, which sustains the SST warming. Such anomalous winds may be amplified by Bjerknes' feedback (Bjerknes 1969), resulting in more precipitation over the equatorial western Indian Ocean and the dateline areas. The anomalous winds also deepen the thermocline in the tropical western Indian Ocean, which helps to sustain the SST warming (Schott et al. 2009; Xie et al. 2002). Compared with CMIP5, the IPWP SST warming simulated by CMIP6 is weaker, related to the shallower thermocline anomalies in CMIP6.

The mixed-layer heat budget in high- and low-skill models

To investigate the underlying mechanisms for IPWP warming biases from the individual model, we have

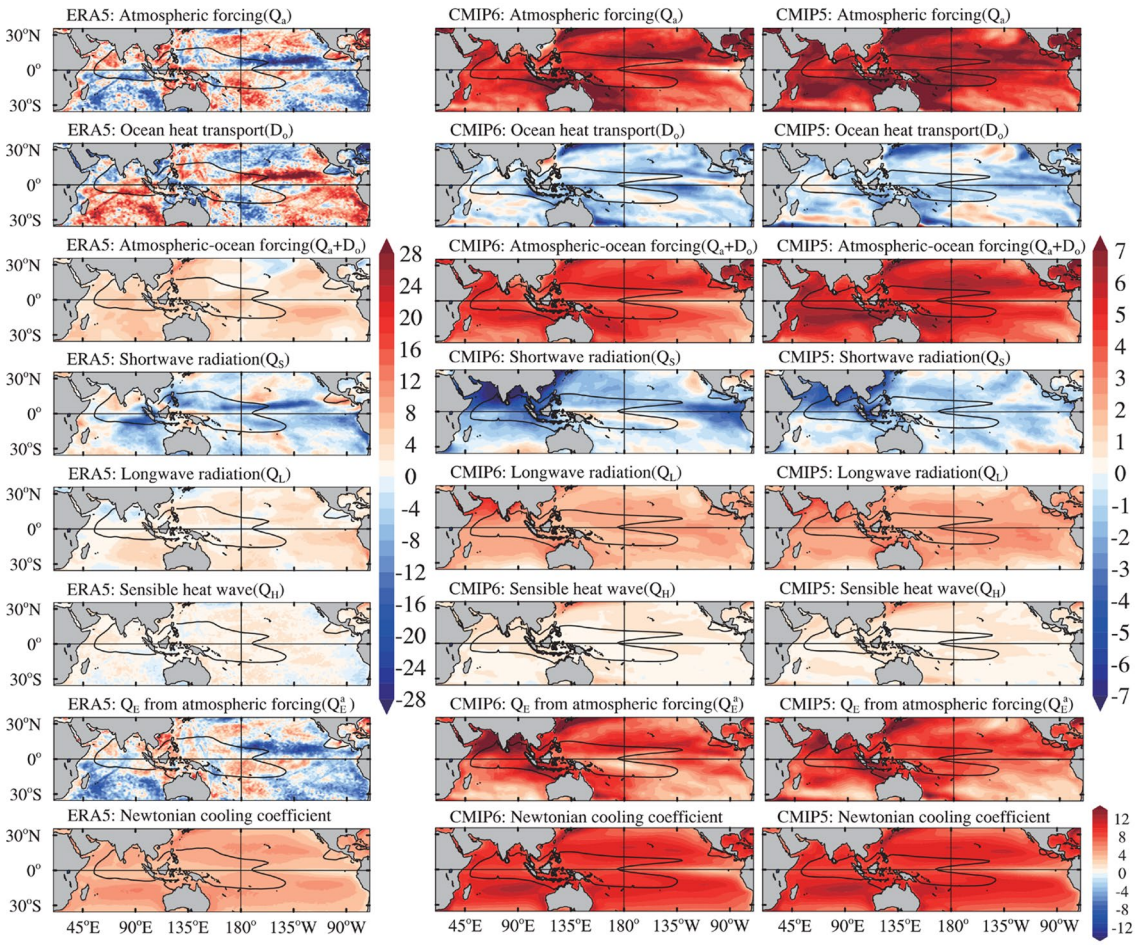

Fig. 3 Linear trends of (top to bottom) atmospheric processes (Q_a), ocean dynamics term (D_O), the sum of atmospheric and oceanic processes ($Q_a + D_o$), the Newtonian cooling coefficient ($\alpha\overline{Q_E}$), net shortwave radiation (Q_S), net longwave radiation (Q_L), sensible heat flux (Q_H), latent heat flux from atmospheric forcing (Q_E^a) from ERA5 (left column), CMIP6 (middle column) and CMIP5 (right column) during 1961–2005. Our convention for warming the ocean is positive. The units of the subfigures are Wm^{-2}/45 yr, except the Newtonian cooling coefficient ($\alpha\overline{Q_E}$, units: $Wm^{-2}K^{-1}$)

Table 1 Linear trends of atmospheric processes (Q_a), ocean dynamics term (D_o), the sum of atmospheric and oceanic processes ($Q_a + D_o$), the Newtonian cooling coefficient ($\alpha\overline{Q_E}$), net shortwave radiation (Q_S), net longwave radiation (Q_L), sensible heat flux (Q_H), latent heat flux from atmospheric forcing (Q_E^a), and wind effect on latent heat flux from atmospheric forcing (Q_E^W) in the Indo-Pacific, Indian, and Pacific warm pool from 1961 to 2005

		ERA5	JRA55	NCEP	CMIP6	CMIP5
Indo-Pacific warm pool	Q_a	1.73	− 5.36	7.24	5.14	6.12
	D_o	3.07	11.07	− 2.55	− 0.7	− 0.58
	$(Q_a + D_o)$	4.8	5.71	4.70	4.44	5.54
	$\alpha\overline{Q_E}$	8.35	9.93	8.22	9.32	9.51
	Q_S	− 3.23	− 7.58	4.73	− 1.62	− 1.6
	Q_L	1.8	2.03	0.61	2.17	2.59
	Q_H	1.34	0.69	0.20	0.5	0.5
	Q_E^a	1.82	− 0.50	1.70	4.09	4.64
	Q_E^W	0.46	− 7.66	− 3.96	0.87	1.11
Indian Ocean warm pool	Q_a	1.8	− 8.11	− 3.26	5.19	6.05
	D_o	3.5	14.48	8.64	− 0.7	− 0.46
	$Q_a + D_o$	5.29	6.37	5.39	4.49	5.59
	$\alpha\overline{Q_E}$	8.09	9.77	8.25	9.13	9.28
	Q_S	− 1.95	− 3.84	2.50	− 3.31	− 2.41
	Q_L	1.05	1.00	1.18	2.5	2.74
	Q_H	1.35	− 0.23	− 0.68	0.65	0.54
	Q_E^a	1.35	− 5.04	− 6.26	5.35	5.18
	Q_E^W	− 2.08	− 18.11	− 2.24	2.01	2.36
Western Pacific warm pool	Q_a	1.7	− 4.09	12.06	5.1	6.17
	D_o	2.88	9.51	− 7.68	− 0.68	− 0.7
	$Q_a + D_o$	4.58	5.41	4.38	4.41	5.47
	$\alpha\overline{Q_E}$	8.47	10.00	8.20	9.38	9.57
	Q_S	− 3.81	− 9.29	5.76	− 0.88	− 1.23
	Q_L	2.15	2.50	0.35	2.03	2.52
	Q_H	1.33	1.12	0.60	0.44	0.48
	Q_E^a	2.04	1.58	5.36	3.51	4.4
	Q_E^W	1.63	− 2.86	− 4.74	0.34	0.41

displayed SST biases due to separate processes in high-skill and low-skill ensemble and their difference (Fig. S6 and S7). CMIP6 high-skill ensemble performs more substantial SST warming in Indian Ocean and weaker magnitude in the Western Pacific Warm Pool than low-skill ensemble (Fig. 5a). The SST trend in IPWP simulated by CMIP5 high-skill ensemble is weaker than that of low-skill ensemble (Fig. 5b). The difference between high- and low-skill scores in SST warming is associated with the difference in the sum of atmospheric and oceanic processes (Fig. 5c and d).

The warmer SST change in the Indian Ocean Warm Pool in the CMIP6 high-skill ensemble is due to the warming effect of more robust atmospheric processes via latent heat flux and weaker ocean dynamics term cooling effect. The warming effect of atmospheric processes in the Western Pacific Warm Pool in the CMIP6 high-skill ensemble is still stronger but offset by a more substantial cooling effect of ocean dynamics term, causing the sum of atmospheric and oceanic processes to be closer to the low-skill ensemble. The weaker SST change in IPWP in the CMIP5 high-skill ensemble is due to the weaker warming effect of atmospheric processes and the more robust cooling effect of ocean dynamics term (Table S3).

Besides, the differences in wind anomalies between high- and low-skill ensembles are mainly concentrated in the equatorial eastern Indian Ocean and tropical western Pacific in CMIP6 and only in the tropical west Pacific in CMIP5, which are consistent with the distribution of anomalies precipitation pattern (Fig. 5e and f). The anomalies of deepened thermocline difference are located in the southwestern Indian Ocean in CMIP6; the anomalies of deepened thermocline difference occupied most of the Indian Ocean in CMIP5 (Fig. 5g and h). Compared with the CMIP6 low-skill ensemble, the distributions of precipitation and sea surface height anomalies

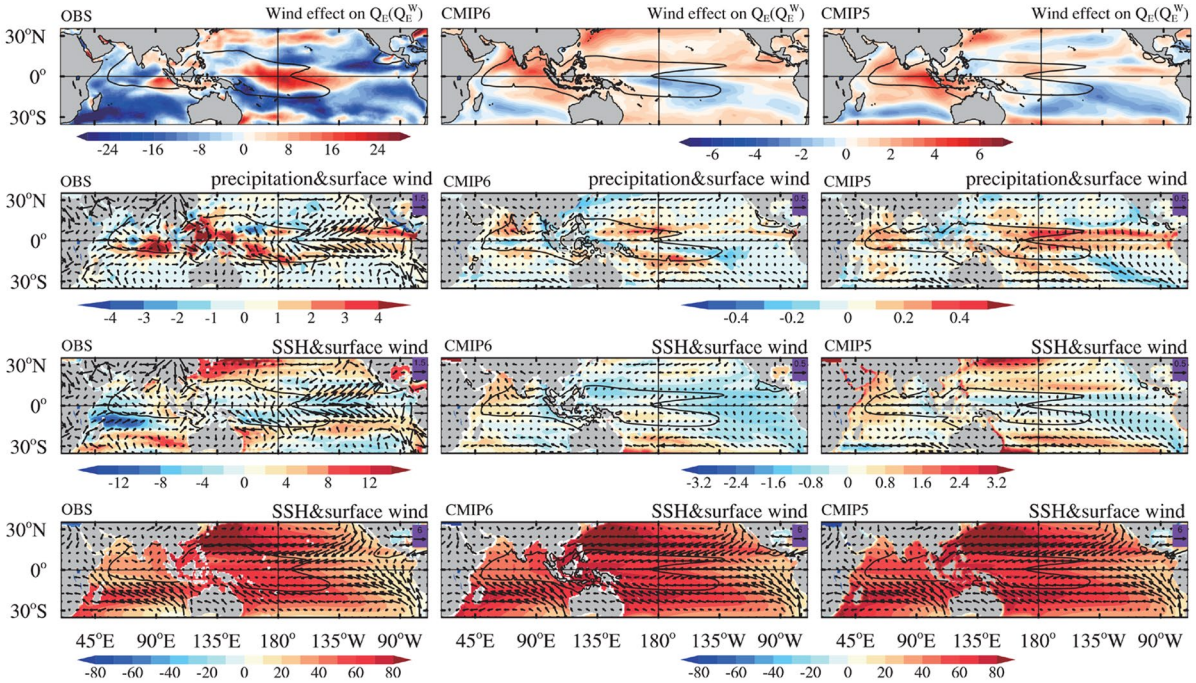

Fig. 4 The linear trends of (top to bottom) wind effect on latent heat flux from atmospheric forcing (Q_E^W), precipitation (shading, mm d^{-1}/45yr), sea surface height (shading, cm/45 yr) and surface wind (vectors, m s^{-1}/45yr) from observation (left column), CMIP6 (middle column) and CMIP5 (right column) during 1961–2005. The climatological sea surface height (shading, cm) and surface wind (vectors, m s^{-1}) during 1961–2005 are shown in the bottom row

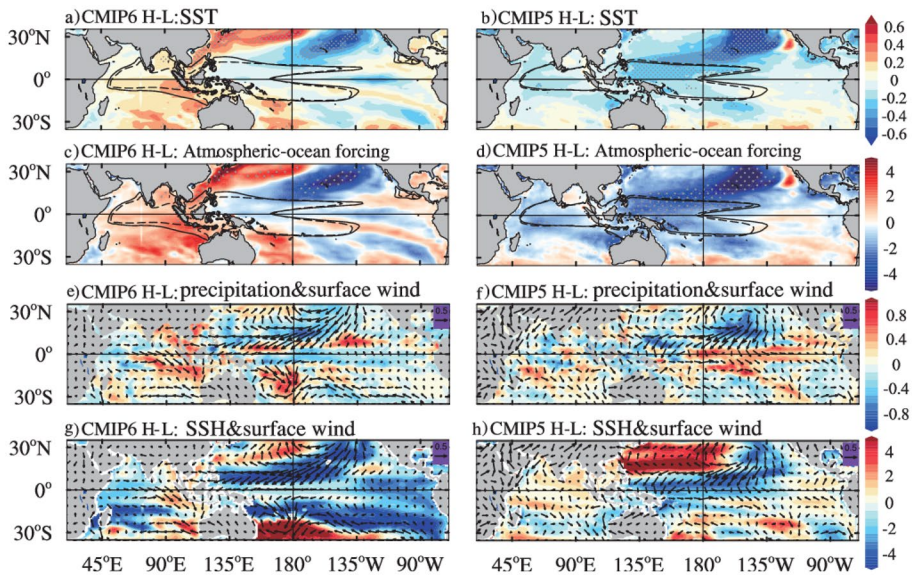

Fig. 5 The difference between high and low skill scores in CMIP6 (left column) and CMIP5 (right column) models. **a** and **b** Represent the linear trend of SST (℃/45 yr). **c** and **d** Represent the linear trend of the sum of atmospheric and oceanic processes ($Q_a + D_o$), Wm^{-2}/45 yr). **e** and **f** Represent the linear trends of precipitation (shading, mm d^{-1}/45yr) and surface wind (vectors, m s^{-1}/45 yr). **g** and **h** Represent the linear trends of sea surface height (shading, cm/45 yr) and surface wind (vectors, m s^{-1}/45 yr)

in the CMIP6 high-skill ensemble are closer to observations, resulting in the warming trend in the tropical Southern Indian Ocean closer to observations (Figs. S8 and S9).

Conclusions

This study evaluates the models' ability to simulate the IPWP warming from CMIP6 and CMIP5. The fundamental physical mechanisms and the causes of model biases for IPWP warming are also discussed. The main conclusions are as follows:

From the perspective of the ensemble mean, models can reproduce observed IPWP warming trends but underestimate the warming magnitude, especially in CMIP6. The observed IPWP warming trend is 0.34 °C/45 yr, while the corresponding CMIP6 MME and CMIP5 MME are 0.26 °C/45 yr and 0.29 °C/45 yr, respectively. Regarding the simulation in the magnitude and spatial pattern of Indo-Pacific warming, the skill scores are higher in CMIP6 MME (0.39) and top models (0.82) than those in CMIP5 (0.14 and 0.76), which is tightly linked to their better performance in simulating associated physical processes in CMIP6.

The decomposition of SST changes shows that the IPWP warming in observations is primarily attributed to the combined effects of atmospheric processes and ocean dynamics term; in contrast, the IPWP warming in models is primarily attributed to atmospheric processes. The model biases and the inter-model differences of IPWP warming are mainly related to the radiative flux and latent heat flux from atmospheric forcing, which can be attributed to the biases of wind fields. The IPWP warming in observation is related to the convergence of low-level wind fields and deeper thermocline in the maritime continental region. However, the climatological easterly wind in the northern Indian Ocean is weakened, suppressing surface evaporation effectively, reducing the latent heat flux from the ocean to the atmosphere, and helping to maintain SST warming. Besides, models tend to simulate the spatially uniform basin-wide warming, which causes the low PCC. This is chiefly because the atmospheric processes and ocean dynamics term are favorable to basin-wide warming, with maxima located in the off-equatorial zones of about 10° S–20° S and 10° N–20° N, which is offset due to the large climatological latent heat flux, leading to the spatially uniform basin-wide warming.

Compared with CMIP5 models, the Indo-Pacific warm pool SST warming simulated by CMIP6 models is weaker, related to the less robust atmospheric processes and the shallower thermocline anomalies affected by CMIP6. The warming trend in the tropical Southern Indian Ocean in the CMIP6 high-skill ensemble is closer to observations due to the improvements in distributions of precipitation and sea surface height anomalies.

Abbreviations

IPWP	Indo-Pacific warm pool
SST	Sea surface temperature
CMIP6	Coupled Model Intercomparison Project phase 6
CMIP5	Coupled Model Intercomparison Project phase 5
MME	Multi-model ensemble
RMSE	Root mean square error
PCC	Pattern correlation coefficients
ERSST	Extended reconstructed SST
HadISST	Hadley Centre Sea Ice and SST
COBESST	Centennial in situ observation based estimates SST

Supplementary Information

The online version contains supplementary material available at https://doi.org/10.1186/s40562-024-00346-6.

Supplementary Material 1.

Acknowledgements

The authors are sincerely grateful to the anonymous reviewers for their valuable comments on this paper.

Author contributions

H. L. Liu initiated and led this research. W. R. Bai conceived the idea, performed the analysis, and wrote the manuscript. All authors participated in discussions during this study and contributed to the writing and revising the manuscript.

Funding

This study was supported by the National Key R&D Program for Developing Basic Sciences (2022YFC3104802), the National Natural Science Foundation of China (U2242214, 42065003), the Strategic Priority Research Program of the Chinese Academy of Sciences (XDB42010404), the Taishan Scholar Program (Grant No. tstp20231237) and the Natural Science Research Project of Shaanxi Province (Grant No. 2023-JC-YB-252).

Availability of data and materials

HadISST data set can be accessed at Met Office Hadley Centre (https://www.metoffice.gov.uk/hadobs/). COBESST, ERSSTv5, and NCEP-NCAR Reanalysis 1 data sets can be accessed at the NOAA/OAR/ESRL PSD website (https://www.esrl.noaa.gov/psd/data/gridded/). ERA-Interim can be accessed at ECMWF (https://apps.ecmwf.int/datasets/). All the CMIP6 model outputs analyzed in this study can be accessed at the Earth System Grid Federation (ESGF) server (https://esgf-node.llnl.gov/projects/esgf-llnl/). All the large ensembles except MPI-ESM are downloaded from the Multi-Model Large Ensemble Archive (https://www.cesm.ucar.edu/projects/community-projects/MMLEA/). The MPI-ESM large ensemble data are available at the MPI Grand Ensemble project website (https://esgf-data.dkrz.de/search/mpi-ge/).

Declarations

Competing interests

The authors declare no competing interests.

Received: 21 March 2024 Accepted: 7 June 2024
Published online: 26 June 2024

References

Bai W, Liu H, Lin P, Shijian H, Wang F (2022) Indo-Pacific warm pool present warming attribution and future projection constraint. Environ Res Lett 17(5):054026. https://doi.org/10.1088/1748-9326/ac5edf

Banks HT, Bindoff NL (2003) Comparison of observed temperature and salinity changes in the Indo-Pacific with results from the coupled climate model HadCM3. Process Mech J Clim 16(1):156–166
Bjerknes J (1969) Atmospheric teleconnections from the equatorial Pacific. Mon Weather Rev 97(3):162–172
Bock L, Lauer A, Schlund M, Barreiro M, Bellouin N, Jones C, Meehl GA, Predoi V, Roberts MJ, Eyring V (2020) Quantifying progress across different CMIP phases with the ESMValTool. J Geophys Res Atmos 125(21):e2019JD032321
Cai W, Cowan T (2013) Why is the amplitude of the Indian Ocean Dipole overly large in CMIP3 and CMIP5 climate models? Geophys Res Lett 40(6):1200–1205
Clement AC, Seager R, Murtugudde R (2005) Why are there tropical warm pools? J Clim 18(24):5294–5311
Cravatte S, Delcroix T, Zhang D, McPhaden M, Leloup J (2009) Observed freshening and warming of the western Pacific Warm Pool. Clim Dyn 33(4):565–589
Du Y, Xie SP (2008) Role of atmospheric adjustments in the tropical Indian Ocean warming during the 20th century in climate models. Geophys Res Lett 35(8):L08712
Eyring V, Bony S, Meehl GA, Senior C, Stevens B, Stouffer RJ, Taylor KE (2016) Overview of the coupled model intercomparison project phase 6 (CMIP6) experimental design and organization. Geosci Model Dev 9(5):1937–1958
Flato G, Marotzke J, Abiodun B, Braconnot P, Chou SC, Collins W, et al (2014) Evaluation of climate models. In Climate change 2013: the physical science basis.: Contribution of Working Group I to the Fifth Assessment Report of the Intergovernmental Panel on Climate Change, p. 741–866
Hayashi M, Shiogama H, Emori S, Ogura T, Hirota N (2021) The Northwestern Pacific Warming Record in August 2020 occurred under anthropogenic forcing. Geophys Res Lett 48(1):e2020GL090956
Hersbach H, Bell B, Berrisford P, Hirahara S, Horányi A, Muñoz-Sabater J, Nicolas J, Peubey C, Radu R, Schepers D, Simmons A, Soci C, Abdalla S, Abellan X, Balsamo G, Bechtold P, Biavati G, Bidlot J, Bonavita M, Chiara G, Dahlgren P, Dee D, Diamantakis M, Dragani R, Flemming J, Forbes R, Fuentes M, Geer A, Haimberger L, Healy S, Hogan RJ, Hólm E, Janisková M, Keeley S, Laloyaux P, Lopez P, Lupu C, Radnoti G, Rosnay P, Rozum I, Vamborg F, Villaume S, Thépaut JN (2020) The ERA5 global reanalysis. Q J R Meteorol Soc 146(730):1999–2049
Hirahara S, Ishii M, Fukuda Y (2014) Centennial-scale sea surface temperature analysis and its uncertainty. J Clim 27(1):57–75
Hirota N, Takayabu YN, Watanabe M, Kimoto M (2011) Precipitation reproducibility over tropical oceans and its relationship to the double ITCZ problem in CMIP3 and MIROC5 climate models. J Clim 24(18):4859–4873
Hu D, Wu L, Cai W, Gupta AS, Ganachaud A, Qiu B, Gordon AL, Lin X, Chen Z, Hu S, Wang G, Wang Q, Sprintall J, Qu T, Kashino Y, Wang F, Kessler WS (2015) Pacific western boundary currents and their roles in climate. Nature 522(7556):299–308
Hu S, Hu D, Guan C, Xing N, Li J, Feng J (2017) Variability of the western Pacific warm pool structure associated with El Niño. Clim Dyn 49(7–8):2431–2449
Jin C, Liu H, Lin P (2023) Evaluation of the seasonal to decadal variability in dynamic sea level simulations from CMIP5 to CMIP6. Geosci Lett. https://doi.org/10.1186/s40562-023-00291-w
Kalnay E, Kanamitsu M, Kistler R, Collins W, Deaven D, Gandin L et al (1996) The NCEP/NCAR 40-year reanalysis project. Bull Am Meteorol Soc 77(3):437–472
Kim ST, Yu J-Y, Lu M-M (2012) The distinct behaviors of Pacific and Indian Ocean warm pool properties on seasonal and interannual time scales. J Geophys Res Atmos 117(5):05128
Kobayashi S, Ota Y, Harada Y, Ebita A, Moriya M, Onoda H, Onogi K, Kamahori H, Kobayashi C, Endo H, Miyaoka K, Takahashi K (2015) The JRA-55 reanalysis: General specifications and basic characteristics. J Meteorol Soc Jpn 93(1):5–48
Kug J-S, Pathirana G, Wu Y-K, Kwon M (2023) Intermodel relation between present-day warm pool intensity and future precipitation changes. Clim Dyn 17:054026
Li J, Su J (2020) Comparison of Indian Ocean warming simulated by CMIP5 and CMIP6 models. Atmos Ocean Sci Lett 13(6):604–611
Li G, Xie S-P (2012) Origins of tropical-wide SST biases in CMIP multi-model ensembles. Geophys Res Lett 39(22):L22703
Li G, Xie S-P, Du Y (2015) Monsoon-induced biases of climate models over the tropical Indian Ocean. J Clim 28(8):3058–3072
Li G, Xie S-P, Du Y, Luo Y (2016) Effects of excessive equatorial cold tongue bias on the projections of tropical Pacific climate change. Part I: the warming pattern in CMIP5 multi-model ensemble. Clim Dyn 47(12):3817–3831
Lindzen RS, Nigam S (1987) On the role of sea surface temperature gradients in forcing low-level winds and convergence in the tropics. J Atmos Sci 44(17):2418–2436
Liu X, Grise KM (2023) Implications of warm pool bias in CMIP6 models on the Northern Hemisphere Wintertime Subtropical Jet and Precipitation. Geophys Res Lett. https://doi.org/10.1029/2023GL104896
Ma X, Jing Z, Chang P, Liu X, Montuoro R, Small RJ, Bryan FO, Greatbatch RJ, Brandt P, Wu D, Lin X, Wu L (2016) Western boundary currents regulated by interaction between ocean eddies and the atmosphere. Nature 535(7613):533–537
Marathe S, Terray P, Karumuri A (2021) Tropical Indian Ocean and ENSO relationships in a changed climate. Clim Dyn 56(9–10):3255–3276
McKenna S, Santoso A, Sen Gupta A, Taschetto AS, Cai W (2020) Indian Ocean Dipole in CMIP5 and CMIP6: characteristics, biases, and links to ENSO. Sci Rep 10(1):1–13
Numaguti A (1995) Dynamics and energy balance of the Hadley circulation and the tropical precipitation zones Part II: sensitivity to meridional SST distribution. J Atmos Sci 52(8):1128–1141
Park IH, Yeh SW, Min SK, Son SW (2021) Emergent constraints on future expansion of the Indo-Pacific warm pool. Geophys Res Lett 49(1):e2021GL097343
Picaut J, Ioualalen M, Menkes C, Delcroix T, McPhaden MJ (1996) Mechanism of the zonal displacements of the Pacific warm pool: Implications for ENSO. Science 274(5292):1486–1489
Randall DA, Wood RA, Bony S, Colman R, Fichefet T, Fyfe J, et al (2007) Climate models and their evaluation. In Climate change 2007: the physical science basis. Contribution of Working Group I to the Fourth Assessment Report of the IPCC (FAR), p. 589–662
Rao SA, Dhakate AR, Saha SK, Mahapatra S, Chaudhari HS, Pokhrel S, Sahu SK (2012) Why is Indian Ocean warming consistently? Clim Change 110(3–4):709–719
Rayner NA, Parker DE, Horton EB, Folland CK, Alexander LV, Rowell DP, Kent EC, Kaplan A (2003) Global analyses of sea surface temperature, sea ice, and night marine air temperature since the late nineteenth century. J Geophys Res Atmos 108(D14):4407
Roxy MK, Dasgupta P, McPhaden MJ, Suematsu T, Zhang C, Kim D (2019) Twofold expansion of the Indo-Pacific warm pool warps the MJO life cycle. Nature 575(7784):647–651
Schneider EK, Fan M (2012) Observed Decadal North Atlantic Tripole SST Variability. Part II: diagnosis of mechanisms. J Atmos Sci 69(1):51–64
Schott FA, Xie S-P, McCreary JP (2009) Indian Ocean circulation and climate variability. Rev Geophys 47(1):RG1002
Seager R, Vecchi GA (2010) Greenhouse warming and the 21st century hydroclimate of southwestern North America. Proc Natl Acad Sci 107(50):21277–21282
Si W, Liu H, Zhang X, Zhang M (2021) Double intertropical convergence zones in coupled ocean-atmosphere models: progress in CMIP6. Geophys Res Lett. https://doi.org/10.1029/2021GL094779
Smith TM, Reynolds RW, Peterson TC, Lawrimore J (2008) Improvements to NOAA's historical merged land-ocean surface temperature analysis (1880–2006). J Clim 21(10):2283–2296
Spencer RW (1993) Global oceanic precipitation from the MSU during 1979–91 and comparisons to other climatologies. J Clim 6(7):1301–1326
Sun Y, Sun DZ, Wu LX, Wang F (2013) Western Pacific warm pool and ENSO asymmetry in CMIP3 models. Adv Atmos Sci 30(3):940–953
Taylor KE (2001) Summarizing multiple aspects of model performance in a single diagram. J Geophys Res Atmos 106(D7):7183–7192
Taylor KE, Stouffer RJ, Meehl GA (2012) An overview of CMIP5 and the experiment design. Bull Am Meteorol Soc 93(4):485–498
Trenberth KE, Fasullo JT (2009) Global warming due to increasing absorbed solar radiation. Geophys Res Lett 36(7):L07706

Wang GJ, Cai WJ, Santoso A (2017) Assessing the impact of model biases on the projected increase in frequency of extreme positive Indian Ocean dipole events. J Clim 30(8):2757–2767
Wang G, Cai W, Santoso A (2021) Simulated thermocline tilt over the tropical Indian Ocean and its influence on future sea surface temperature variability. Geophys Res Lett 48(6):e2020GL091902
Weller E, Min SK, Cai W, Zwiers FW, Kim YH, Lee D (2016) Human-caused Indo-Pacific warm pool expansion. Sci Adv 2(7):e1501719
Wienders N, Arhan M, Mercier H (2000) Circulation at the western boundary of the South and Equatorial Atlantic: exchanges with the ocean interior. J Mar Res 58(6):1007–1039
Williams AP, Funk C (2011) A westward extension of the warm pool leads to a westward extension of the Walker circulation, drying eastern Africa. Clim Dyn 37(11–12):2417–2435
Wyrtki K (1989) Some thoughts about the west Pacific warm pool. In Proceedings of the western pacific international meeting and workshop on TOGA COARE, New Caledonia: ORSTOM/Nouméa, p 99–109
Xie SP, Annamalai H, Schott FA, McCreary JP (2002) Structure and mechanisms of South Indian Ocean climate variability. J Clim 15(8):864–878
Xie SP, Deser C, Vecchi GA, Ma J, Teng HY, Wittenberg AT (2010) Global warming pattern formation: sea surface temperature and rainfall. J Clim 23(4):966–986
Yang Y, Wang F, Zheng J (2020) CMIP5 model biases in the climatological mean state of the western Pacific warm pool. Theor Appl Climatol 140(1–2):533–545
Yao S-L, Huang G, Wu R-G, Qu X, Chen D (2016) Inhomogeneous warming of the Tropical Indian Ocean in the CMIP5 model simulations during 1900–2005 and associated mechanisms. Clim Dyn 46(1–2):619–636
Ying J, Huang P (2016) Cloud–radiation feedback as a leading source of uncertainty in the tropical Pacific SST warming pattern in CMIP5 models. J Clim 29(10):3867–3881
Zhang R, Wang X, Wang C (2018) On the simulations of global oceanic latent heat flux in the CMIP5 multimodel ensemble. J Clim 31(17):7111–7128
Zhang Q, Liu B, Li S, Zhou T (2023a) Understanding models' global sea surface temperature bias in mean state: from CMIP5 to CMIP6. Geophys Res Lett 50(4):e2022GL100888
Zhang R, Guo W, Wang X, Wang C (2023b) Ambiguous variations in tropical latent heat flux since the years around 1998. J Clim 36(10):3403–3415
Zuo H, Balmaseda MA, Mogensen K (2017) The new eddy-permitting ORAP5 ocean reanalysis: description, evaluation and uncertainties in climate signals. Clim Dyn 49(3):791–811

Publisher's Note